NANO LETTERS
Letter
pubs.acs.org/NanoLett

High Performance and Bendable Few-Layered InSe Photodetectors with Broad Spectral Response

Srinivasa Reddy Tamalampudi,[†,∥,#,○] Yi-Ying Lu,[†,‡,○] Rajesh Kumar U.,[†,‡,#] Raman Sankar,[§] Chun-Da Liao,[†,‡] Karukanara Moorthy B.,[⊥,#] Che-Hsuan Cheng,[†,‡] Fang Cheng Chou,[§] and Yit-Tsong Chen*[,†,‡]

[†]Institute of Atomic and Molecular Sciences, Academia Sinica, Taipei 106, Taiwan

[‡]Department of Chemistry and [§]Center for Condensed Matter Sciences, National Taiwan University, No. 1, Sec. 4, Roosevelt Road, Taipei 106, Taiwan

[∥]Department of Physics, National Central University, Jung-Li 320, Taiwan

[⊥]Department of Engineering and System Science, National Tsing Hua University, Hsinchu 30013, Taiwan

[#]Taiwan International Graduate Program, Academia Sinica, Taipei 106, Taiwan

Supporting Information

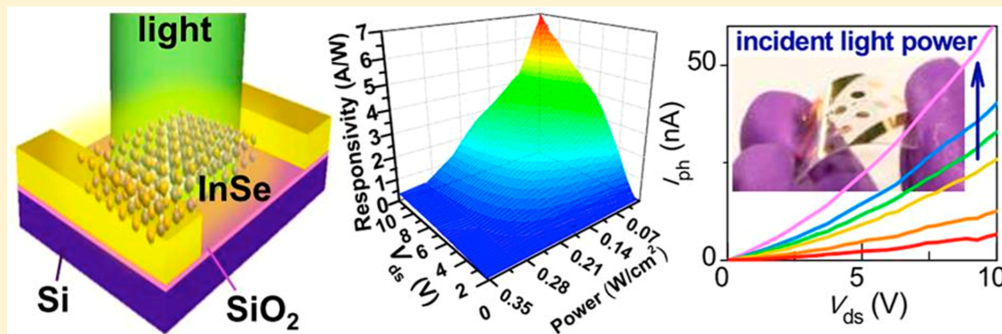

ABSTRACT: Two-dimensional crystals with a wealth of exotic dimensional-dependent properties are promising candidates for next-generation ultrathin and flexible optoelectronic devices. For the first time, we demonstrate that few-layered InSe photodetectors, fabricated on both a rigid SiO_2/Si substrate and a flexible polyethylene terephthalate (PET) film, are capable of conducting broadband photodetection from the visible to near-infrared region (450−785 nm) with high photoresponsivities of up to 12.3 AW^{-1} at 450 nm (on SiO_2/Si) and 3.9 AW^{-1} at 633 nm (on PET). These photoresponsivities are superior to those of other recently reported two-dimensional (2D) crystal-based (graphene, MoS_2, GaS, and GaSe) photodetectors. The InSe devices fabricated on rigid SiO_2/Si substrates possess a response time of ∼50 ms and exhibit long-term stability in photoswitching. These InSe devices can also operate on a flexible substrate with or without bending and reveal comparable performance to those devices on SiO_2/Si. With these excellent optoelectronic merits, we envision that the nanoscale InSe layers will not only find applications in flexible optoelectronics but also act as an active component to configure versatile 2D heterostructure devices.

KEYWORDS: *Indium selenide, two-dimensional materials, flexible photodetectors, transistor, responsivity*

Two-dimensional (2D) crystals have emerged as a new class of materials for next-generation ultrathin and flexible optoelectronic devices, including optical sensors, solar cells, and light-emitting diodes, because of their unique dimensional-dependent properties.[1] For transistor applications, the planar geometry of 2D crystals not only facilitates device integration with standard semiconductor technology[2] but also allows the reduction of channel length,[3] which would be difficult to achieve for low-dimensional materials, such as quantum dots and nanowires. Graphene, being the first prototype of 2D crystals as the channel material in photodetectors, can offer a broad spectral detection and ultrafast sensing due to its linear energy dispersion.[4] However, the intrinsically weak light absorption (∼2.3% for pristine graphene) and short photo-carrier lifetime of graphene lead to poor photoresponsivity (5×10^{-4} AW^{-1}, as listed in Table S1 of the Supporting Information) and internal quantum efficiency (6−16%, Table S1 of the Supporting Information).[4] Moreover, the gapless nature of graphene yields high dark current and results in no clear on-and-off states, which are crucial in both photodetection and power consumption.[5] While several strategies to address these issues through band structure engineering[6] and absorption efficiency enhancement of graphene are ongoing,[7,8]

Received: March 4, 2014
Revised: April 8, 2014
Published: April 17, 2014

© 2014 American Chemical Society

another approach that is rapidly emerging is to explore the optoelectronic properties of semiconducting 2D crystals as alternative channel materials, such as transition metal dichalcogenides (TMDCs)[9] and group IVA metal chalcogenides.[10] As a recent example, the monolayer MoS_2 photodetector was reported to be able to reach an enhanced photoresponsivity of 7.5×10^{-3} AW^{-1} via the application of a back-gate voltage (V_g) at 50 V.[11] Moreover, by adjusting the number of layers in TMDC crystals, intriguing optical properties, such as an indirect to direct band gap transition, an increase in band gap energy (E_g), Van Hove singularities in the electronic density of states, and valley polarization, have been discovered in group VIB TMDCs (MoS_2, $MoSe_2$, WS_2, and WSe_2), which are essential for realization of highly efficient, advanced optoelectronic devices.[12,13] However, the optoelectronic properties of other members in the 2D family are still in their early stages of exploration, and new findings in photodetection performance as well as the diversities of spectral range can be anticipated.

Indium selenide (InSe), belonging to the group IIIA–VIA layered semiconductors (MX, M = Ga and In, X = S, Se, and Te), has gained renewed interests due to its anisotropic optical, electronic, and mechanical properties with targeting applications in memory devices, optical sensors, and thermoelectric implements.[14,15] Recent studies revealed that few-layered GaS and GaSe photodetectors with the spectral window in the ultraviolet (UV) region exhibit photoresponsivity of 4.2 and 2.8 AW^{-1}, respectively.[16,17] Compared with GaS ($E_g \approx 3.05$ eV) and GaSe ($E_g \approx 2.1$ eV), bulk InSe has a narrower direct bandgap[18] ($E_g \approx 1.3$ eV) yet one that overlaps well with the solar spectrum, thus offering a broader spectral response than those of GaS and GaSe. In contrast to GaS and the group VIB TMDCs, layered InSe undergoes a crossover transition from direct to indirect band gap as the layer thickness is reduced to $\leq$6 nm.[19] Furthermore, InSe has stronger quantum confinement than those of the other group IIIA–VIA family because of its narrower band gap and smaller exciton reduced mass,[19] allowing the controllability of the band gap for spectrally tunable nanodevices within a single material system. A very recent report shows that few-layered InSe photodetectors fabricated on SiO_2/Si substrates possess a photoresponse of 34.7 mAW^{-1} at 532 nm,[20] which is about 3 orders of magnitude lower than that of our devices. Such difference could stem from the appropriate preservation of the intrinsic properties of InSe in our devices, which were fabricated via a photoresist-free process. Note that 2D crystal is mainly made up of its surface and thus is sensitive to environmental perturbations.

In this work, we present a comprehensive study of high performance few-layered InSe photodetectors fabricated on both a rigid SiO_2/Si substrate and a flexible polyethylene terephthalate (PET) film. This is the first demonstration that few-layered InSe is capable of conducting broadband photodetection from the visible to near-infrared region (450–785 nm) with high photoresponsivities of up to 12.3 AW^{-1} at 450 nm (on SiO_2/Si) and 3.9 AW^{-1} at 633 nm (on PET), which are superior to those of other reported 2D crystal-based (graphene, MoS_2, GaS, and GaSe) photodetectors (Table S1 of the Supporting Information). Remarkably, the photoresponsivity of few-layered InSe photodetector built on the SiO_2/Si substrate can be further enhanced to 157 AW^{-1} (at $\lambda = 633$ nm) simply by applying a back-gate voltage to 70 V. The few-layered InSe channel exhibits the n-type characteristics of a field-effect transistor (FET) with a carrier mobility of ~0.1 $cm^2\ V^{-1}\ s^{-1}$. Taking a step further, the photoresponsivity and photoswitching stability of the InSe device on the flexible PET film were examined with and without bending, of which the measured data are comparable to those on a rigid SiO_2/Si substrate. The crystal growth of InSe flakes and subsequent device fabrication and device characterization are described in the experimental section of the Supporting Information.

InSe is a layered crystal arranged in a hexagonal lattice (Figure 1a) consisting of four close-packed monatomic sheets

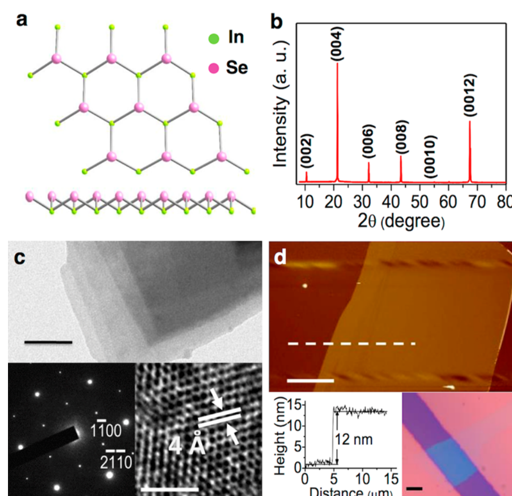

Figure 1. Characterization of the as-grown InSe crystals and few-layered InSe nanosheets. (a) Top and side views of the hexagonal structure of InSe crystal. (b) XRD spectrum of the as-grown InSe crystal. (c) TEM image (top panel, with a scale bar of 50 nm), SAED pattern (bottom left), and HR-TEM image (bottom right, with a scale bar of 2 nm) of few-layered InSe nanosheets. (d) AFM image of the InSe channel of a photodetector (top panel, with a scale bar of 5 μm). The height profile (bottom left) depicts a scan along the white dashed line in the top panel, indicating the InSe layers are ~12 nm in thickness. Optical image of the as-fabricated InSe photodetector (bottom right, with a scale bar of 5 μm).

in the sequence of Se–In–In–Se and therefore can be mechanically exfoliated using the scotch tape method used for graphene. The crystallographic phase of the as-grown InSe crystal was determined by X-ray diffraction (XRD), as shown in Figure 1b. The XRD pattern was indexed to a hexagonal structure with the lattice constants of $a = 4.005$ Å and $c = 16.64$ Å (JCPDS-34-1431).[21] The thickness of the monolayer InSe can be estimated to be ~8 Å from the lattice constants ($c/2$).[19] The morphology and chemical composition of the InSe flakes were characterized by scanning electron microscopy (SEM) and energy-dispersive X-ray spectroscopy (EDS), where the SEM image exhibits a typical nanosheet-like morphology (Figure S1a of the Supporting Information) and the EDS elemental map indicates the homogeneous indium and selenium contents in InSe (Figure S1a of the Supporting Information) and reveals that the stoichiometric ratio of In and Se is ~1:1 (Figure S1c of the Supporting Information). In Figure 1c, the crystalline structure of InSe flakes was further characterized by transmission electron microscopy (TEM), high resolution (HR)-TEM, and selected-area electron diffraction (SAED) to confirm the nanosheet-like geometry, hexagonal structure, and high crystallinity of the InSe flakes. The SAED pattern with the incident beam along [0001] direction (c-axis) is shown in the bottom left of Figure 1c. The

clear Bragg spots of ⟨1$\bar{1}$00⟩ and ⟨2$\bar{1}\bar{1}$0⟩ indicate the single crystallinity of our as-grown InSe crystal. The lattice constant along the *a* or *b* axis is 4 Å as revealed from the HR-TEM image (bottom right image of Figure 1c) and is consistent with previous results.[22] In Figure 1d, the thickness of the as-fabricated few-layered InSe photodetector (with its optical image shown in the bottom right) was determined by atomic force microscopy (AFM) to be ∼12 nm, corresponding to ∼14 layers of InSe; meanwhile, thinner InSe layers of ∼2.5 nm in thickness were also achieved (Figure S2 of the Supporting Information). Raman spectra of InSe flakes of different thicknesses with excitation at 532 nm are depicted in Figure S3 of the Supporting Information. The three Raman peaks observed at 117, 176, and 228 cm^{-1}, corresponding to the A^1_{1g}, E^1_{2g}, and A^2_{1g} modes, respectively, are in accord with those of previously reported bulky InSe.[23]

We first probed the electronic transport in few-layered InSe by using a back-gated FET configuration as schematically illustrated in the bottom panel of Figure 2a. The drain-source

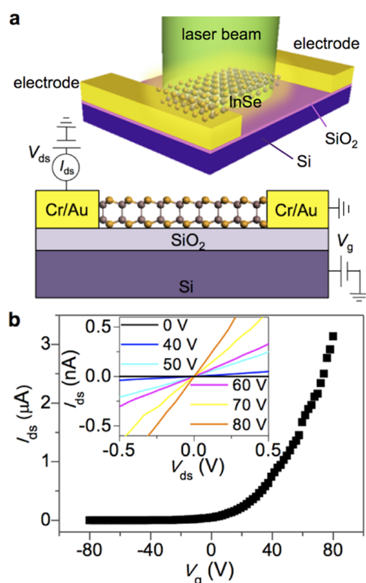

Figure 2. Transfer characteristics of a few-layered InSe-FET. (a) The schematic illustrations represent a few-layered InSe-FET under optoelectronic investigation (top panel) and electrical measurement (bottom panel). (b) The transfer curve of a few-layered InSe-FET was measured by scanning V_g from −80 to 80 V at V_{ds} = 10 V. (top inset) The linear I_{ds}−V_{ds} curves obtained at V_g values from 0 to 80 V indicate ohmic contact.

current vs bias voltage (I_{ds}−V_{ds}) curves measured at various back-gate voltages (V_g from 0 to 80 V, shown in the inset of Figure 2b) are linear, indicating good ohmic contact between the Au electrodes and InSe channel. Figure 2b plots the I_{ds} as a function of back-gate voltage (I_{ds}−V_g) swept from +80 to −80 V at V_{ds} = 10 V. The few-layered InSe channel exhibits the same n-type semiconductive nature as bulky InSe crystals due to the generation of Se vacancies during the crystal growth.[24] The effective field-effect electron mobility (μ_e) of the few-layered InSe-FET extracted from the transfer curve in the linear regime can be estimated using the equation $\mu_e = (L/WCV_{ds})(dI_{ds}/dV_g)$, where $C = \varepsilon_0\varepsilon_r/d$ (with ε_r = 3.9 and d = 300 nm being the relative permittivity and thickness of the insulating SiO_2 layer) is the capacitance per unit area estimated for gate dielectrics, L ≈ 11 μm is the channel length, and W ≈ 19 μm is the channel width. The calculated field-effect electron mobility of our device is ∼0.1 cm^2 V^{-1} s^{-1} and the on/off ratio is ∼10^4, which are comparable to those of the recently reported GeS- and GeSe-FETs.[25]

Next, we demonstrated the sensitive photoresponsivity of our few-layered InSe photodetector illuminated under various intensities and wavelengths. Figure 3a shows the illumination

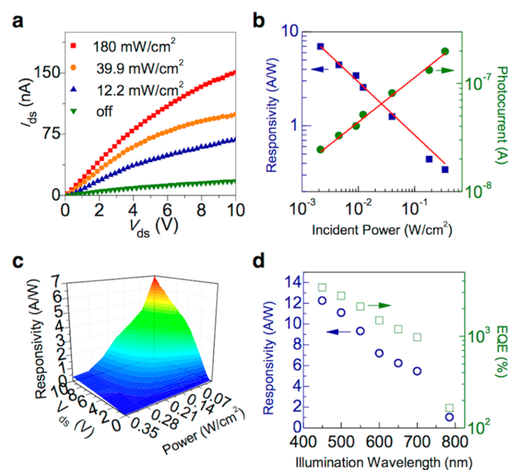

Figure 3. Optoelectronic characterization of a few-layered InSe photodetector on a rigid SiO_2/Si substrate. (a) Typical output curves of a few-layered InSe photodetector acquired in the dark and with illumination at various excitation intensities (180, 39.9, and 12.2 mW cm^{-2}) at V_g = 0 V. (b) Photocurrent (green solid dots) and responsivity (blue solid squares) as a function of illumination intensity at V_{ds} = 10 V and V_g = 0 V. The power laws of $R \approx P^{-0.56}$ and $I_{ph} \approx P^{0.41}$ were determined from fitting the measured data. (c) A 3D responsivity map of the few-layered InSe photodetector. (d) Spectral responsivity (R) and calculated external quantum efficiency (EQE) of the InSe device illuminated at 450−785 nm with excitation intensities of 0.66 (at 450 nm), 0.92, 0.96, 0.70, 0.69, 0.72, and 15.1 mW cm^{-2} (at 785 nm).

intensity dependence of the output (I_{ds}−V_{ds}) curves excited at 633 nm with a He−Ne laser under illumination intensities of 180, 39.9, and 12.2 mW cm^{-2} and in the dark. Under intense illumination, more electron−hole pairs were generated in InSe via the band-to-band transition, where the photoinduced electrons and holes were swept to electrodes in different directions guided by the drain−source electric field, resulting in more channel current. To analyze the quantitative dependence of the photoresponse on the illumination intensity, the photocurrent ($I_{ph} = I_{light} - I_{dark}$) was measured at V_{ds} = 10 V as a function of the laser power density (P). We observed that the photocurrent increases sublinearly following a power law of $I_{ph} \approx P^{0.41}$, as shown in Figure 3b (green solid dots). The trap states, caused by the defects and/or charged impurities present in InSe and the adsorbed molecules at InSe-SiO_2/Si interface,[26] might account for the laser power dependence, where more traps could be filled by photoinduced charge carriers as the light intensity increases, leading to the final saturation of the photocurrent. This phenomenon was also observed previously in MoS_2 photodetectors.[9,27]

One critical figure-of-merit to determine the performance of the few-layered InSe photodetector is its responsivity ($R = I_{ph}/PS$), defined as the ratio of the generated photocurrent (I_{ph}) in response to optical power density (P) impinging on the detector (S, illuminated area).[28] Figure 3b presents the

responsivity (blue solid squares) as a function of illumination power density of $R \approx P^{-0.56}$ (solid red line). Remarkably, the responsivity of our InSe device reaches ~7 AW^{-1} at the illumination intensity of 2.1 mW cm^{-2} at λ = 633 nm, which is 4 orders of magnitude higher than those of MoS_2 phototransistors (4.2 × 10^{-4} AW^{-1}) and graphene photodetectors (5 × 10^{-4} AW^{-1}, λ = 1550 nm).[4,11] In addition, another important parameter of external quantum efficiency (EQE), the number ratio of electrons flowing out of the device in response to impinging photons, can also be estimated to be ~1367% (P = 2.1 mW cm^{-2}, λ = 633 nm, and V_{ds} = 10 V), where EQE = $hcR/e\lambda$, h is Planck's constant, c is the light velocity, R is the responsivity, e is the elementary electronic charge, and λ is the excitation wavelength. The other criterion is specific detectivity (D^*), reflecting the photodetector's sensitivity, and can be expressed as $D^* = RS^{1/2}/(2eI_{dark})^{1/2}$ because the primary source of noise to limit D^* is the shot noise from dark current.[29] Under illumination of 633 nm and P = 2.1 mW cm^{-2} at V_{ds} = 10 V, the calculated D^* is 1.07 × 10^{11} Jones, which is comparable to both InGaAs[30] and solution-processed nanocrystalline Bi_2S_3[31] photodetectors. In Figure 3c, a 3D responsivity map of our InSe device clearly shows that the responsivity can also be tuned by adjusting the drain-source voltage (V_{ds}), where an increasing V_{ds} can shorten the carriers' transit time by providing a stronger electric field to govern the photoinduced carriers reaching the electrodes, thus reducing the possibility of recombination.

To further test the photoresponse characteristics, we determined the spectral responsivity of our InSe device under illuminating monochromatic light of 450−785 nm measured at V_{ds} = 10 V and V_g = 0 V, as shown in Figure 3d. The responsivity increases up to 12.3 AW^{-1} as the photon energy increases to 2.75 eV (450 nm) and is generally in line with the tendency along the absorption spectrum of InSe.[32] In contrast to the recently reported MoS_2-, GaS-, and GaSe-based photodetectors, our few-layered InSe device offers high responsivity in a broader spectral range from visible to near-infrared. The calculated EQE for each excitation wavelength is also plotted in Figure 3d. A list of the performance metrics for comparison among the recently developed 2D crystal-based photodetectors is provided in Table S1 of the Supporting Information.

We now explore the dependence of the current profile on the back-gate voltage (V_g) in the InSe channel. The bottom panel of Figure 4a presents a comparison of I_{ds} as a function of V_g recorded at V_{ds} = 10 V under illumination (λ = 633 nm and P = 350 mW cm^{-2}) and in the dark, with a schematic energy band diagram illustrating the generation and extraction of the photoinduced charge carriers. Under illumination, I_{ds} remains higher than that in the dark for all applied V_g values from −20 to 80 V and increases notably when V_g is higher than the threshold voltage (V_{th}). These observations can be realized that, without illumination and a bias voltage, the device reached its equilibrium state when the Fermi levels of both Au (~5.1 eV) and InSe (~4.4 eV)[33] are aligned, resulting in small Schottky barriers. When applying a back-gate voltage of $V_g < V_{th}$ (condition I, top left panel of Figure 4a), the down-shifted Fermi level of InSe results in a larger energy barrier between the conduction band of InSe and the Fermi level of Au. Therefore, upon illumination, the photocurrent in the InSe channel outnumbered the tunneling and thermionic current. In contrast, at $V_g > V_{th}$ (condition II, top right panel of Figure 4a), the tunneling and thermionic current can easily overcome the

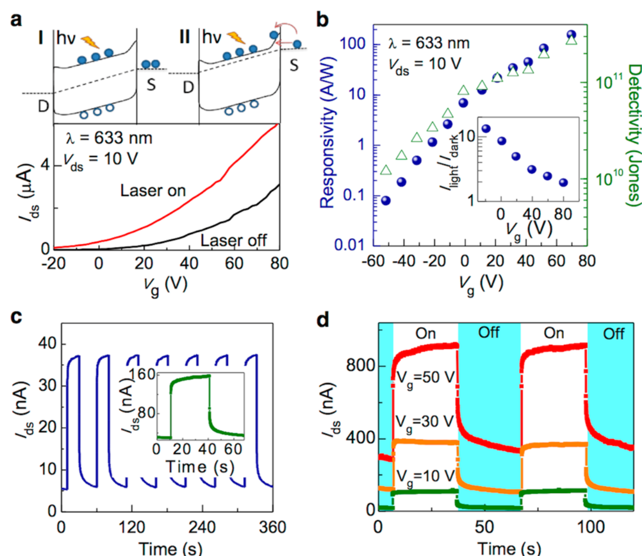

Figure 4. V_g dependence and temporal response of the photocurrent. (a,top) Energy band diagrams of a few-layered InSe under illumination at (I) $V_g < V_{th}$ and (II) $V_g > V_{th}$. (a, bottom) Comparison of the transfer curves of a few-layered InSe photodetector measured in the dark and under illumination at λ = 633 nm and P = 350 mW cm^{-2}. (b) The responsivity and calculated specific detectivity as a function of V_g recorded at V_{ds} = 10 V under illumination of λ = 633 nm and P = 2.1 mW cm^{-2}. (inset) Photoresponse ratio (I_{light}/I_{dark}) as a function of V_g. (c) A test of the photoswitching stability for the InSe device in response to a train of pulsed illumination at λ = 633 nm, P = 350 mW cm^{-2}, and V_{ds} = 2.0 V. (inset) Temporal response of the InSe device measured under illumination of λ = 633 nm, P = 350 mW cm^{-2}, and V_{ds} = 7.0 V. (d) The photocurrents acquired at V_g of 10, 30, and 50 V under pulsed illumination at λ = 633 nm and P = 350 mW cm^{-2}.

barrier because the Fermi level of InSe approached its conduction band.[34] The photoresponse ratio (I_{light}/I_{dark}, shown in the inset of Figure 4b) demonstrates that more tunneling and thermionic current participate in the InSe channel as V_g increases. Figure 4b further plots the responsivity as a function of V_g under illumination (λ = 633 nm and P = 2.1 mW cm^{-2}); remarkably, the responsivity significantly increases from 6.9 to 157 AW^{-1} when V_g is swept from 0 to 70 V and almost vanishes as V_g is set to −60 V. Such gate-tunable responsivity by adjusting the Schottky barriers is an imperative feature for the pixelated imaging applications.

As demonstrated in Figure 4c, our InSe device maintains the long-term stability of its photoresponse in a series of periodical light stimulations. The high reproducibility of photocurrents in the photoswitching is also sustained at different V_{ds} of 1, 3, 5, and 7 V (Figure S4 of the Supporting Information). In the inset of Figure 4c, we also recorded the dynamic response of our device during the on-and-off switching of an incident light with a better temporal resolution. While the rising time is measured to take ~40−50 ms, the falling time contains two components with a fast decay of ~50−60 ms (corresponding to the earlier 50% decrease) and a slow relaxation of 4 s (in the later half decline). The response times of our InSe device are comparable to those obtained by other layered semiconductor-based photodetectors (e.g., GaSe, GaS, and MoS_2, as listed in Table S1 of the Supporting Information).[16,17,11] Such a relatively long photocarriers lifetime (decay time), compared with traditional metal−semiconductor−metal photodetectors,[35] supports the existence of the aforementioned trap states, which could be

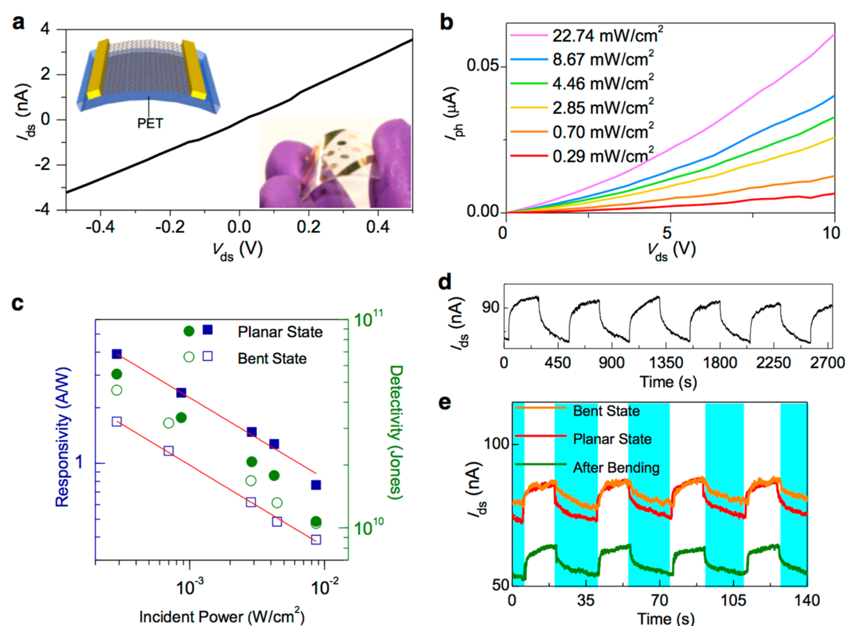

Figure 5. Optoelectronic characterization of a flexible photodetector. (a) The $I_{ds}-V_{ds}$ curve of the few-layered InSe photodetector on PET measured in the dark. (top inset) Schematic illustration of a few-layered InSe photodetector on a PET substrate. (bottom inset) A digital image of the as-fabricated flexible InSe device on PET. (b) The photocurrent of the InSe device on PET film acquired when the device was in planar geometry with 633 nm illumination of 22.74, 8.67, 4.46, 2.85, 0.70, and 0.29 mW cm^{-2}. (c) The responsivity and calculated specific detectivity as a function of the illumination intensity acquired in both planar and bent states at V_{ds} = 10 V. The red solid lines were fitted to the experimental data with the power law of $R \approx P^{-0.44}$ in both states. (d) A test of the photoswitching stability for the flexible InSe device in response to a train of pulsed illumination at λ = 633 nm, P = 15 mW cm^{-2}, and V_{ds} = 10 V. (e) The photoresponse curves were measured for the comparison of dynamic photoswitching when the InSe device was of planar geometry, in a bent state, and after bending.

exacerbated further due to the high surface-to-volume ratio of 2D InSe. These traps could capture holes to delay the recombination of a free electron–hole pair in consequence of a single photon absorption. As a result, this electron with prolonged lifetime can make several effective transits in the InSe channel between electrodes (once this electron is collected by the drain, a replenishing one will be injected from the source) due to charge conservation.[36] Together with efficient light absorption due to the direct band gap nature in few-layered InSe (>6 nm in thickness), high EQE InSe photodetectors can thus be achieved. Furthermore, we observed that the photocurrent decays slower at higher V_g, as shown in Figure 4d. This scenario could be ascribed to the water molecules adsorbed on the InSe device, which are inclined to bind the silanol groups on the SiO_2 surface[37] because water molecules are easily subject to the electric field's alignment/orientation by applying V_g due to their high dipole moment (~1.8 D). Under higher V_g, highly oriented/aligned water molecules could induce an increased density of trap states,[38] resulting in a broader distribution of relaxation lifetimes. Thus, the high-speed response of a photodetector can be realized by improving the substrate surface via modification/passivation to screen the unnecessary effect from polar/charged impurities.

Finally, we investigate the optoelectronic performance of bendable InSe devices. A schematic illustration and a photograph of the as-fabricated InSe device on a PET substrate are depicted in the top and bottom insets of Figure 5a, respectively, demonstrating the device's mechanical flexibility. Similar to the InSe device fabricated on a rigid SiO_2/Si substrate, this bendable photodetector also holds an ohmic contact between the InSe channel and Au electrodes, as confirmed by the $I_{ds}-V_{ds}$ measurement (Figure 5a). The light-intensity-dependent photocurrents recorded in both the planar and bent states are shown in Figure 5b and Figure S5a of the Supporting Information, respectively, and can be fitted with the power law (Figure S5b of the Supporting Information), exhibiting similar behavior as the devices on the SiO_2/Si substrates. To compare the InSe device performance on PET without and with bending (a bending radius of 3 cm), Figure 5c plots the responsivity and the corresponding specific detectivity as a function of the illumination intensity. In the bent state, although the responsivity is reduced by approximately half compared with the unbent state, the responsivity reaches ~1.7 AW^{-1} (P = 0.28 mW cm^{-2} at 633 nm) and is substantially higher than the values for graphene (5 × 10^{-4} AW^{-1}) and MoS_2 (4.2 × 10^{-4} AW^{-1}) based photodetectors. The reduced responsivity in the bent state is likely due to the crack formation in metal electrodes,[39] resulting in the degradation of photocarriers collection efficiency. The strain built in the bent state could also reduce responsivity because of the alterations of band structure in the few-layered InSe and its corresponding optical properties.[40] In the measurements with a light intensity of 0.28 mW cm^{-2} at 633 nm and V_{ds} = 10 V, the estimated specific detectivities of D^* = 5.47 × 10^{10} and 4.58 × 10^{10} Jones for the unbent and bent states, respectively, are comparable. Moreover, the bendable photodetectors also exhibit a highly stable photoresponse (Figure 5d) to a train of periodical light stimulation (P = 15 mW cm^{-2} at 633 nm) for up to ~45 min. As shown in Figure S6 of the Supporting Information, we repeated these experiments on another bendable InSe device and confirmed the similar device performance. In Figure 5e, we compared the dynamic photoswitching of our flexible device for three conditions of planar geometry, bent state, and after bending (then measured at planar geometry) under irradiation with a 633 nm laser at 15 mW cm^{-2}, where high

reproducibilities of on-and-off switching are observed for all three conditions. These results reveal that the stretchable nature of 2D InSe nanosheets is responsible for the excellent features of stability and reproducibility, suggesting that these nanosheets are suitable for advanced optoelectronic applications.

In summary, few-layered InSe photodetectors on a rigid SiO_2/Si substrate with high responsivity over a broad spectral range at 450−785 nm are demonstrated for the first time. The high responsivity (12 AW^{-1} under illumination of $\lambda = 450$ nm and $P = 0.66$ mW cm^{-2}) and broad spectral detection (from visible to near-infrared) are superior to other recently developed 2D crystals (graphene, MoS_2, GaS, and GaSe)-based photodetectors. The responsivity of the back-gated InSe device can be enhanced significantly from 6.9 to 157 AW^{-1} simply by applying V_g. The flexible photodetectors of few-layered InSe manufactured on a PET film also exhibit comparable device performance to those fabricated on a rigid SiO_2/Si substrate. The few-layered InSe photodetectors, produced on both rigid and flexible substrates, exhibit low dark current and long-term stability in photoswitching. With such excellent optoelectronic merits, we envision that the nanoscale InSe layers will become not only a superb candidate to construct advanced appliances of optical sensing and low power consumption FETs but also an active component to configure versatile 2D heterostructure devices.

■ ASSOCIATED CONTENT

Supporting Information

Growth of single crystalline InSe flakes, the fabrication and characterization of few-layered InSe devices, Figures S1−S6, and Table S1. This material is available free of charge via the Internet at http://pubs.acs.org.

■ AUTHOR INFORMATION

Corresponding Author

*(Y.T.C.) E-mail: ytcchem@ntu.edu.tw.

Author Contributions

○Y.-Y.L. and S.R.T. contributed equally to this work.

Notes

The authors declare no competing financial interest.

■ ACKNOWLEDGMENTS

We thank Dr. Satender Katari, Mr. T. Venkatesh, and M. Rajesh Kumar for their help with the Raman and XRD measurements. This work was partially supported by the National Science Council of Taiwan under NSC 101-2113-M-002-0016-MY2, 101-2119-M-002-007, and 102-2627-M-002-001. Y.-Y.L. was supported by a postdoctoral fellowship from Academia Sinica. Technical support from NanoCore, the Core Facilities for Nanoscience and Nanotechnology at Academia Sinica, is acknowledged.

■ REFERENCES

(1) Bonaccorso, F.; Sun, Z.; Hasan, T.; Ferrari, A. C. *Nat. Photonics* **2010**, *4*, 611−622.

(2) Rogers, J. A.; Lagally, M. G.; Nuzzo, R. G. *Nature* **2011**, *477*, 45−53.

(3) Butler, S. Z.; Hollen, S. M.; Cao, L.; Cui, Y.; Gupta, J. A.; Gutiérrez, H. R.; Heinz, T. F.; Hong, S. S.; Huang, J.; Ismach, A. F.; et al. *ACS Nano* **2013**, *7*, 2898−2926.

(4) Xia, F.; Mueller, T.; Lin, Y.-M.; Valdes-Garcia, A.; Avouris, P. *Nat. Nanotechnol.* **2009**, *4*, 839−843.

(5) Wang, X.; Cheng, Z.; Xu, K.; Tsang, H. K.; Xu, J.-B. *Nat. Photonics* **2013**, *7*, 888−891.

(6) Avouris, P. *Nano Lett.* **2010**, *10*, 4285−4294.

(7) Konstantatos, G.; Badioli, M.; Gaudreau, L.; Osmond, J.; Bernechea, M.; de Arquer, F. P. G.; Gatti, F.; Koppens, F. H. L. *Nat. Nanotechnol* **2012**, *7*, 363−368.

(8) Koppens, F. H. L.; Chang, D. E.; García de Abajo, F. J. *Nano Lett.* **2011**, *11*, 3370−3377.

(9) Lopez-Sanchez, O.; Lembke, D.; Kayci, M.; Radenovic, A.; Kis, A. *Nat. Nanotechnol.* **2013**, *8*, 497−501.

(10) Perea-López, N.; Elías, A. L.; Berkdemir, A.; Castro-Beltran, A.; Gutiérrez, H. R.; Feng, S.; Lv, R.; Hayashi, T.; López-Urías, F.; Ghosh, S.; et al. *Adv. Funct. Mater.* **2013**, *23*, 5511−5517.

(11) Yin, Z.; Li, H.; Li, H.; Jiang, L.; Shi, Y.; Sun, Y.; Lu, G.; Zhang, Q.; Chen, X.; Zhang, H. *ACS Nano* **2011**, *6*, 74−80.

(12) Britnell, L.; Ribeiro, R. M.; Eckmann, A.; Jalil, R.; Belle, B. D.; Mishchenko, A.; Kim, Y.-J.; Gorbachev, R. V.; Georgiou, T.; Morozov, S. V.; et al. *Science* **2013**, *340*, 1311−1314.

(13) Wang, Q. H.; Kalantar-Zadeh, K.; Kis, A.; Coleman, J. N.; Strano, M. S. *Nat. Nanotechnol.* **2012**, *7*, 699−712.

(14) Camara, M. O. D.; Mauger, A.; Devos, I. *Phys. Rev. B* **2002**, *65*, 125206.

(15) Olguín, D.; Rubio-Ponce, A.; Cantarero, A. *Eur. Phys. J. B* **2013**, *86*, 1−9.

(16) Hu, P.; Wang, L.; Yoon, M.; Zhang, J.; Feng, W.; Wang, X.; Wen, Z.; Idrobo, J. C.; Miyamoto, Y.; Geohegan, D. B.; et al. *Nano Lett.* **2013**, *13*, 1649−1654.

(17) Hu, P.; Wen, Z.; Wang, L.; Tan, P.; Xiao, K. *ACS Nano* **2012**, *6*, 5988−5994.

(18) Gomes da Costa, P.; Dandrea, R. G.; Wallis, R. F.; Balkanski, M. *Phys. Rev. B* **1993**, *48*, 14135−14141.

(19) Mudd, G. W.; Svatek, S. A.; Ren, T.; Patanè, A.; Makarovsky, O.; Eaves, L.; Beton, P. H.; Kovalyuk, Z. D.; Lashkarev, G. V.; Kudrynskyi, Z. R.; et al. *Adv. Mater.* **2013**, *25*, 5714.

(20) Lei, S.; Ge, L.; Najmaei, S.; George, A.; Kappera, R.; Lou, J.; Chhowalla, M.; Yamaguchi, H.; Gupta, G.; Vajtai, R.; et al. *ACS Nano* **2014**, *8*, 1263−1272.

(21) Wang, J.-J.; Cao, F.-F.; Jiang, L.; Guo, Y.-G.; Hu, W.-P.; Wan, L.-J. *J. Am. Chem. Soc.* **2009**, *131*, 15602−15603.

(22) Hayashi, T.; Ueno, K.; Saiki, K.; Koma, A. *J. Cryst. Growth* **2000**, *219*, 115−122.

(23) Carlone, C.; Jandl, S.; Shanks, H. R. *Phys. Status Solidi B* **1981**, *103*, 123−130.

(24) Birkmire, R. W.; Eser, E. *AnRMS* **1997**, *27*, 625−653.

(25) Late, D. J.; Liu, B.; Luo, J.; Yan, A.; Matte, H. S. S. R.; Grayson, M.; Rao, C. N. R.; Dravid, V. P. *Adv. Mater.* **2012**, *24*, 3549−3554.

(26) Ghatak, S.; Pal, A. N.; Ghosh, A. *ACS Nano* **2011**, *5*, 7707−7712.

(27) Zhang, W.; Huang, J.-K.; Chen, C.-H.; Chang, Y.-H.; Cheng, Y.-J.; Li, L.-J. *Adv. Mater.* **2013**, *25*, 3456−3461.

(28) Xia, F.; Mueller, T.; Golizadeh-Mojarad, R.; Freitag, M.; Lin, Y.-M.; Tsang, J.; Perebeinos, V.; Avouris, P. *Nano Lett.* **2009**, *9*, 1039−1044.

(29) Gong, X.; Tong, M.; Xia, Y.; Cai, W.; Moon, J. S.; Cao, Y.; Yu, G.; Shieh, C.-L.; Nilsson, B.; Heeger, A. J. *Science* **2009**, *325*, 1665−1667.

(30) Jiang, J.; Tsao, S.; O'Sullivan, T.; Zhang, W.; Lim, H.; Sills, T.; Mi, K.; Razeghi, M.; Brown, G. J.; Tidrow, M. Z. *Appl. Phys. Lett.* **2004**, *84*, 2166−2168.

(31) Konstantatos, G.; Levina, L.; Tang, J.; Sargent, E. H. *Nano Lett.* **2008**, *8*, 4002−4006.

(32) Tu, H.; Kelley, D. F. *Nano Lett.* **2005**, *6*, 116−122.

(33) Sánchez-Royo, J. F.; Pellicer-Porres, J.; Segura, A.; Gilliland, S. J.; Avila, J.; Asensio, M. C.; Safonova, O.; Izquierdo, M.; Chevy, A. *Phys. Rev. B* **2006**, *73*, 155308.

(34) Sze, S. M. *Semiconductor Devices: Physics and Technology*; J. Wiley & Sons: New York, 2001.

(35) Liu, M. Y.; Chen, E.; Chou, S. Y. *Appl. Phys. Lett.* **1994**, *65*, 887−888.

(36) Konstantatos, G.; Badioli, M.; Gaudreau, L.; Osmond, J.; Bernechea, M.; de Arquer, F. P. G.; Gatti, F.; Koppens, F. H. L. *Nat. Nanotechnol.* **2012**, *7*, 363−368.
(37) Kim, W.; Javey, A.; Vermesh, O.; Wang, Q.; Li, Y.; Dai, H. *Nano Lett.* **2003**, *3*, 193−198.
(38) Late, D. J.; Liu, B.; Matte, H. S. S. R.; Dravid, V. P.; Rao, C. N. R. *ACS Nano* **2012**, *6*, 5635−5641.
(39) Lee, G.-H.; Yu, Y.-J.; Cui, X.; Petrone, N.; Lee, C.-H.; Choi, M. S.; Lee, D.-Y.; Lee, C.; Yoo, W. J.; Watanabe, K.; et al. *ACS Nano* **2013**, *7*, 7931−7936.
(40) Conley, H. J.; Wang, B.; Ziegler, J. I.; Haglund, R. F.; Pantelides, S. T.; Bolotin, K. I. *Nano Lett.* **2013**, *13*, 3626−3630.